

Defects depth estimation in a CFRP material by active infrared thermography using neural network

H. HALLOUA^a, A. ELHASSNAOUI^b, A. ZRHAIBA^b, S. KRAIBAA^a, A. OBBADI^a, Y. ERRAMI^a, S. SAHNOUN^a

^aLaboratory of Electronics, Instrumentation and Energetic, Faculty of Sciences, B.P 20. 24000 El Jadida, Morocco

^bIndustrial Engineering Laboratory, Faculty of Science and Technology, BP: 523 Beni Mellal, Morocco

The use of carbon fiber materials is continually increasing in various industrial sectors because of their excellent thermomechanical properties. This work presents the implementation of a new approach based on a neural network for the processing of pulsed thermography data, to determine the internal defects depths in CFRP material. Preprocessing of network training data, using standard thermal contrast and principal component analysis has reduced the number of neural network inputs. The elaborated neural network was tested on simulation data with deviations not exceeding 5%. Experimental validation confirmed the proposed method's effectiveness for evaluating the internal defects depths in CFRP composites.

(Received October 11, 2019; accepted April 9, 2020)

Keywords: Non-destructive Testing, Infrared thermography, neural network, defect depth, carbon fiber reinforced polymers, CFRP

1. Introduction

The use of carbon fiber materials is continually increasing in various industrial sectors. They are more and more used because of their excellent thermomechanical properties, such as their low densities, their high mechanical resistance, good thermal and electrical insulation[1]. However, the performance of carbon fiber reinforced polymers (CFRP) may be affected by defects, such as delamination, cracks, inclusions or inhomogeneities of matter[2]. The precise evaluation of these defects depth has crucial importance in the inspection and maintenance of carbon fiber reinforced polymer parts, used particularly in the aeronautical field. Therefore, it is important to develop effective inspection techniques to control these materials and thus protect people and equipment.

Non-destructive testing (NDT) [3] is an indispensable tool in the expensive materials' quality control. Infrared thermography is commonly used as an effective non-destructive tool in the detection and characterization of internal defects[4]. It is a technique that has the ability to measure the surface temperature distribution of an object remotely. Thus, it allows rapid control of parts and structures on site without having to move or remove them.

In this work, pulsed thermography is used to detect defects in CFRP composites. A neural algorithm is used to estimate different defects depths in a CFRP sample. A principal component analysis [4] is used to reduce the neural network input data in the form of standard thermal contrast [5].

2. Principle of pulsed infrared thermography

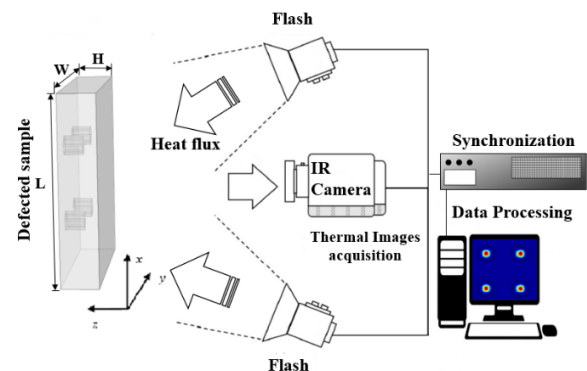


Fig. 1. pulsed infrared thermography principle (color online)

Pulsed infrared thermography is one of the most widely used techniques in non-destructive thermal control [7]. During control, the inspected surface is heated by a thermal pulse, lasting few milliseconds for materials with high thermal conductivities, and few seconds for low thermal conductivities samples. This thermal stimulation generates a temperature gradient which propagates by conduction inside the inspected sample (Figure 1). The sample's thermal response is recorded with an infrared camera to be digitally processed. Thermal data analysis allows the evaluation of thermal conductivity and diffusivity, or the detection and characterization of defects at different depths in the inspected part.

3. Thermal modeling of the studied sample

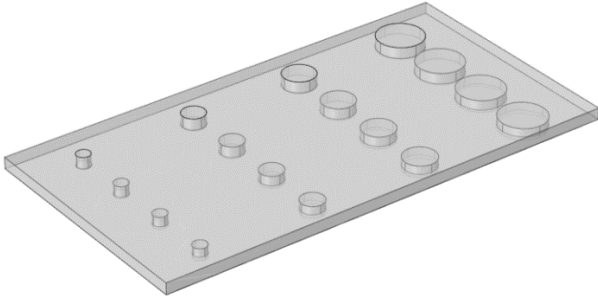


Fig. 2. 3d image of the studied CFRP sheet

The studied sample (

Fig.) is a carbon fiber reinforced polymer sheet (CFRP), with the following geometrical dimensions: a length of $L = 200$ mm, a width of $W = 105$ mm and a thickness $H = 5$ mm. This sheet contains 16 artificial defects located at different depths from the heated face, materializing air inclusions.

We have considered circular defects with the following diameters 6, 10, 14 and 20mm. Their respective thicknesses are 0.25, 0.5, 1.0 and 2.0 mm following a horizontal axis parallel to the length of the sheet. We have reported in Fig. 3 a sketch of a flawed CFRP sheet.

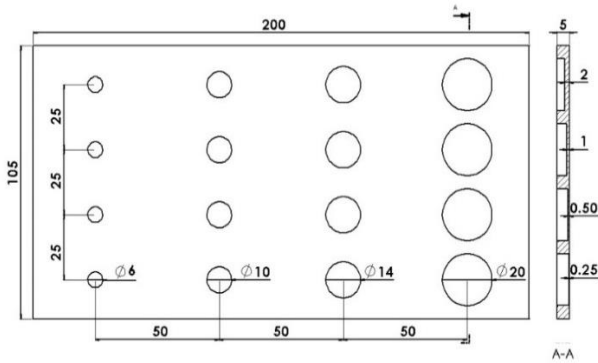


Fig. 3. Sketch of a CFRP sheet with inclusions of different sizes at different depths

3.1. Boundary conditions

We applied an external heat flux $Q = 5 \text{ kW/m}^2$ to heat the controlled sample's upper face for a 10s period. The initial temperature is equal to $T_0 = 293.15 \text{ K}$. The lateral faces are supposed to be perfectly isolated. These conditions are translated by the equations below:

$$T(x, y, z)_{t=0} = T_0 \quad (1)$$

$$Q_{x=0} = Q_{x=L} = 0 \quad (2)$$

$$Q_{y=0} = Q_{y=W} = 0 \quad (3)$$

The conduction heat transfer process in the sample is described by the following differential equation:

$$\rho C_p \left(\frac{\partial T}{\partial t} \right) - \nabla \cdot (k \nabla T) = 0 \quad (4)$$

where ρ is the density, C_p is the thermal capacity of the material, T is the absolute temperature, k is the material's thermal conductivity and t is the time.

The boundary conditions in the upper face of the controlled sheet are described by equation 5:

$$n \cdot (k \nabla T) = h(T_{air} - T) + \sigma \varepsilon (T_{amb}^4 - T^4) + Q \quad (5)$$

where T_{amb} and T_{air} respectively represent the ambient and the air temperatures. ε is the emissivity of the surface, and σ is the Stefan-Boltzmann constant. h denotes the convective heat transfer coefficient of the material, and n the normal direction to the surface. The used thermal properties are presented in Table 1.

Table 1. The thermal properties of the used materials [8]

Parameters	Symbols	Values
Initial temperature [K]	T_0	293.15
Ambient temperature [K]	T_{amb}	293.15
Air temperature [K]	T_{air}	293.15
Density of CFRP [kg m^{-3}]	ρ_{cfRP}	1500
Heat capacity of CFRP [J/(kg.K)]	cp_{cfRP}	1000
CFRP Parallel conductivity [W/(m.K)]	$k_{//}$	7
CFRP Transverse conductivity [W/(m.K)]	k_{\perp}	0.8
Air thermal conductivity [W/(m.K)]	k_a	0.026
Air heat capacity [J/(kg.K)]	cp_a	1005
Air density of [kg m^{-3}]	ρ_a	1.225
heat exchange Coefficient [$\text{Wm}^{-2}\text{k}^{-1}$]	h	9.1
Emissivity	ε	0.98

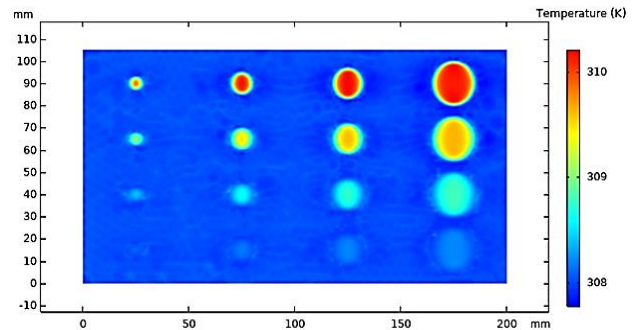


Fig. 4. Thermogram of the sample surface obtained at $t = 11\text{s}$ (color online)

The resolution of the differential equations (1-5) by the finite element method, using the numerical calculation software COMSOL Multiphysics 5.4, allowed us to obtain the thermal distribution of the inspected sheet.

Fig. 4 shows a thermogram of the upper face at time $t = 11s$. We notice the appearance of internal defects in the material. It is noted that defects near the surface and defects of large sizes are the most visible in the thermograms.

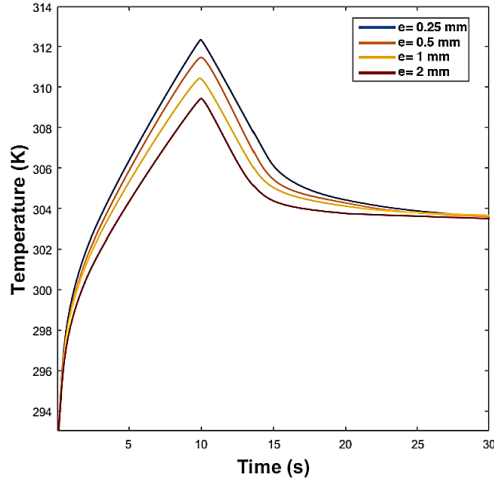


Fig. 5. Temperature variation as a function of time for defects of diameter 6 mm at different depths (color online)

We have reported in

Fig. the temperature variation as a function of time for defects of the same diameter $d = 6$ mm located at different depths $e = 0.25, 0.5, 1$ and 2 mm. We note that the temperature values decrease as the depth of the defect increases.

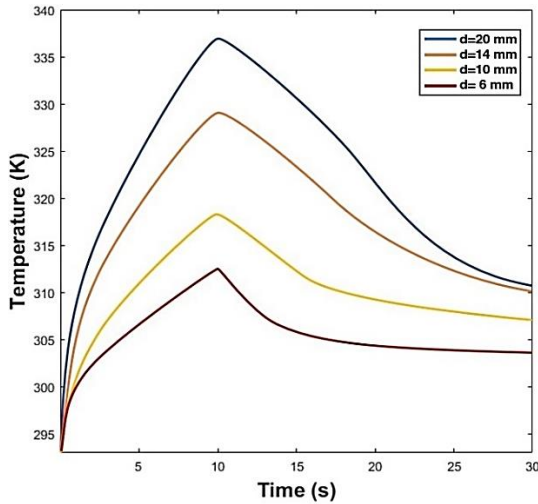


Fig. 6. Temperature variation as a function of time for defects of different diameters located at the same depth $e = 0.25$ mm (color online)

We have reported in figure 6 the temperature variation as a function of time for defects at the same depth $e = 0.25$ mm, of different diameters $d = 6, 10, 14$ and 20 mm. It is noted that the temperature values decrease as the diameter of the defect decreases. In order to increase the degree of precision and to realize a more exhaustive study, we

calculated the standard thermal contrast[6] to eliminate thermal noise, produced by healthy areas in the sample to be tested. It is defined by the relation (6).

$$C_{std}(t) = \frac{T_d(t) - T_d(t_0)}{T_s(t) - T_s(t_0)} \quad (6)$$

With $T_d(t)$ the surface temperature of the defective zone. $T_s(t)$ represents the surface temperature of the healthy zone and t_0 the start time of the stimulation.

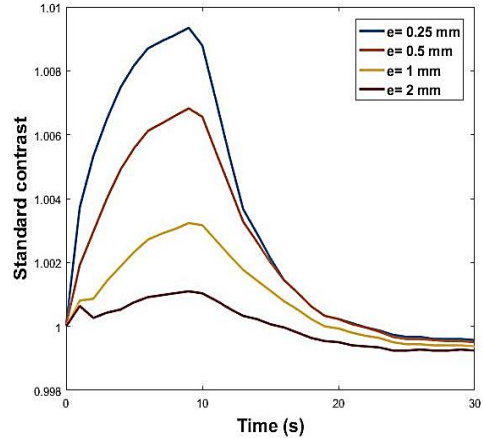


Fig. 7. Standard thermal contrast variation over time for defects located at different depths (color online)

We have reported in Fig. 7 the standard thermal contrast variation as a function of time for defects' depths of 6 mm diameter, located at depths $e = 0.25$ mm, 0.5 mm, 1 mm and 2 mm. We note that the standard contrast helps to better reveal the presence of defects located at different depths in composite materials. To model the relation between the temperature of the controlled surface and the depth of the defects, we will use neural networks that are widely recognized to be able to correlate very complex problems.

3.2. Neural networks

Artificial neural networks [9] are tools for processing information to model complex relationships. They try to reproduce the same behaviors of biological neurons. They are composed of basic units of data processing called formal neurons, interconnected in the form of a network with several layers (Fig. 8).

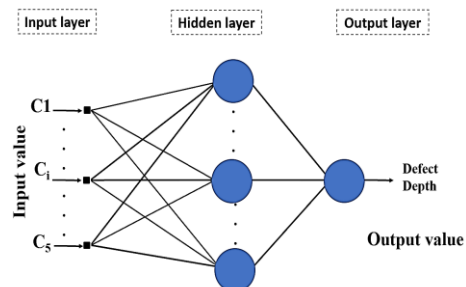


Fig. 8. Three-layer neural network (color online)

The use of artificial neural networks has developed in many disciplines and particularly in the field of non-destructive thermal control[10]. The general work of an artificial neural network is to find the configuration of connection weights between neurons, to associate a good response (outputs) with the inputs. The use of a neural network is done in two stages. The learning phase (modeling) is responsible for establishing values for each of the connections of the network. Then, a phase of use, where the network is presented with input, and it tells us in return the calculated output (established model).

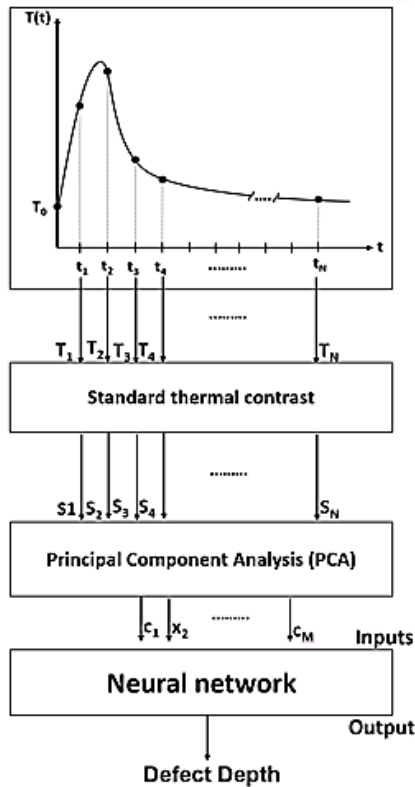


Fig. 9. Schemes of the steps of the proposed neuronal method

In this work, we used the neural network to find a relationship between the surface temperature and the depth of defects in a CFRP sheet. For this purpose, a three-layer neural network (Fig. 8), is used to process the temperatures obtained by the finite element method, to determine the depth of the material's internal defects. Supervised learning was chosen because it is the most suitable for approximating relationships (between temperatures and corresponding depths).

Fig. 9 shows the steps followed in the development of the neuronal model. The first step is to prepare the learning data of the neural network. In our case, the obtained temperatures (T_1, T_2, \dots, T_N) are not used as input to the network, but it is the standard thermal contrast, calculated using the relation (6) over a period of 18 s of the cooling part with a sampling step of 0.1s (that is 181 values).

To reduce the number of entries, and optimize the data provided to the network while keeping the useful information for the learning phase, a principal component

analysis (PCA) is used. This analysis reduced the number of thermal contrast vector data ($s_1, s_2, \dots, s_N=181$) to an input vector, composed of five main components ($c_1, c_2, c_3, c_4, c_M=5$) that correspond to the greatest variance in thermal contrast.

To prepare the learning vectors, we carried out a finite element simulation of a CFRP plate, containing defects with diameters $d = 6\text{mm}$, $d = 10\text{mm}$, $d = 14\text{mm}$, and $d = 20\text{mm}$. The depth of the defects varies between 0.1 mm and 5 mm. We calculated the evolution above each defect for 490 temperature evolutions. To avoid the problem of overfitting, we divided the learning data into three data sets: training, validation, and testing. The training is done with the training set, then evaluations are performed on the validation set to control overfitting. When the learning seems successful, a final evaluation can be performed on the testing set. In our case, we divided the 490 input vectors according to the percentage 70% for the network training set, 15% for the validation set, and 15% for the network testing set[11].

In the design of an artificial neural network, there are a number of parameters to define that can affect the learning of the network, and generally, a lot of experimentation is required. Some of these parameters are the type of neural network that should be considered, the learning algorithm, the number of layers and neurons that define the network architecture. In our case, the Levenberg Marquard algorithm gave better performances in adjusting the neural network's final weights in comparison with the fourteen backpropagation algorithms' results, most used in the training of neural networks. To structure the network, we used a neural network with a single hidden layer with a sigmoidal activation function, this type of architecture is usually sufficient to approximate any nonlinear function[12]. For the hidden layer, we fixed the number of neurons using an incremental approach where we started the learning with a single neuron, then a new neuron was added to the hidden layer each time. we compared the error of the new network ($n + 1$ neurons) with the preceding one (n neurons); the process will stop when adding a new neuron no longer improves accuracy; which makes it possible to reduce the number of neurons.

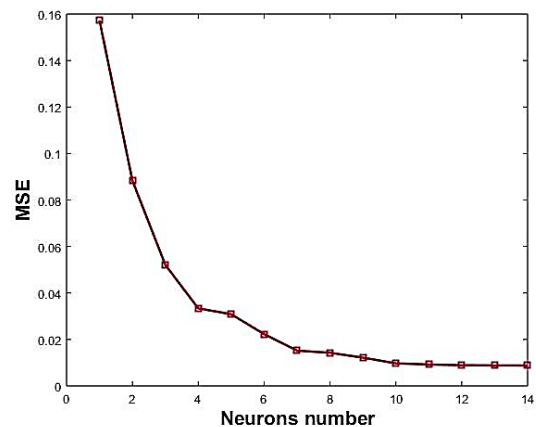


Fig. 10. The neural network performance as a function of the neurons number in the hidden layer (color online)

Fig. 10 shows the results of this incremental study. It shows that the use of twelve neurons in the hidden layer gave better results. The performance of a neural network is evaluated by the value of the mean squared error (MSE) (7) representing the mean squared difference between the depths obtained by the network (output) O_i et the real depths (targets) T_i . The good performances correspond to the low MSE values.

$$MSE = \frac{1}{n} \sum_{i=0}^n (O_i - T_i)^2 \quad (7)$$

4. Results and discussion

We have reported in Fig. 11, the neural network learning results; by plotting the variation of the mean squared error (MSE) obtained during the three phases, training, validation, and test. As can be seen, for the three phases, the mean squared error decreases with the increase of the number of iterations, to reach the best performance ($MSE = 0.000117$) after 188 iterations.

To test our network, we attempted to estimate defect depths with corresponding thermal contrast values with defect depths that were not used in the learning phase. Table 2 shows the estimated results.

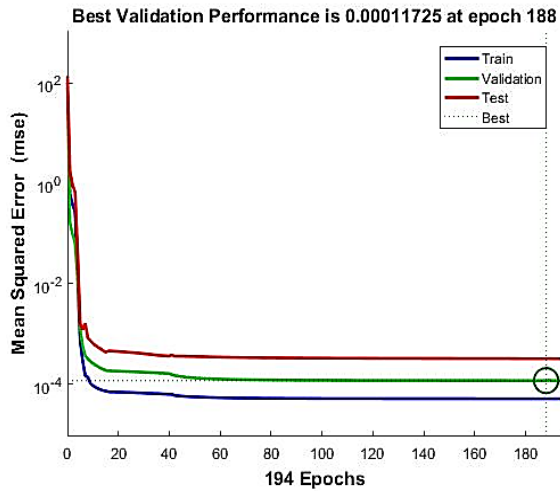


Fig. 11. The mean squared error variation in the learning stage (color online)

Table 2. Comparison between depth values estimated by our neural network and target depths

Test #	Target value (mm)	Estimated values (mm)	Gap (%)
1	0.22	0.214	3
2	0.45	0.429	5
3	0.62	0.593	3
4	0.85	0.868	2
5	1.25	1.189	5

We note that the estimated depths by the neural network are close to the target values with a gap that does not exceed 5%. Following these encouraging results, a validation with experimental results is necessary to confirm the robustness of the established neuronal model in order to estimate the depths of defects that exist in industrial sites.

In order to apply the developed neuronal model above to experimental results, we used the experimental data (Fig. 12) corresponding to the temperature variation during the pulsed thermography control of a CFRP sheet, containing 3 defects located at depths of $e = 0.25$ mm curve (a), $e = 0.5$ mm curve (b) and $e = 1$ mm curve (c) [8].

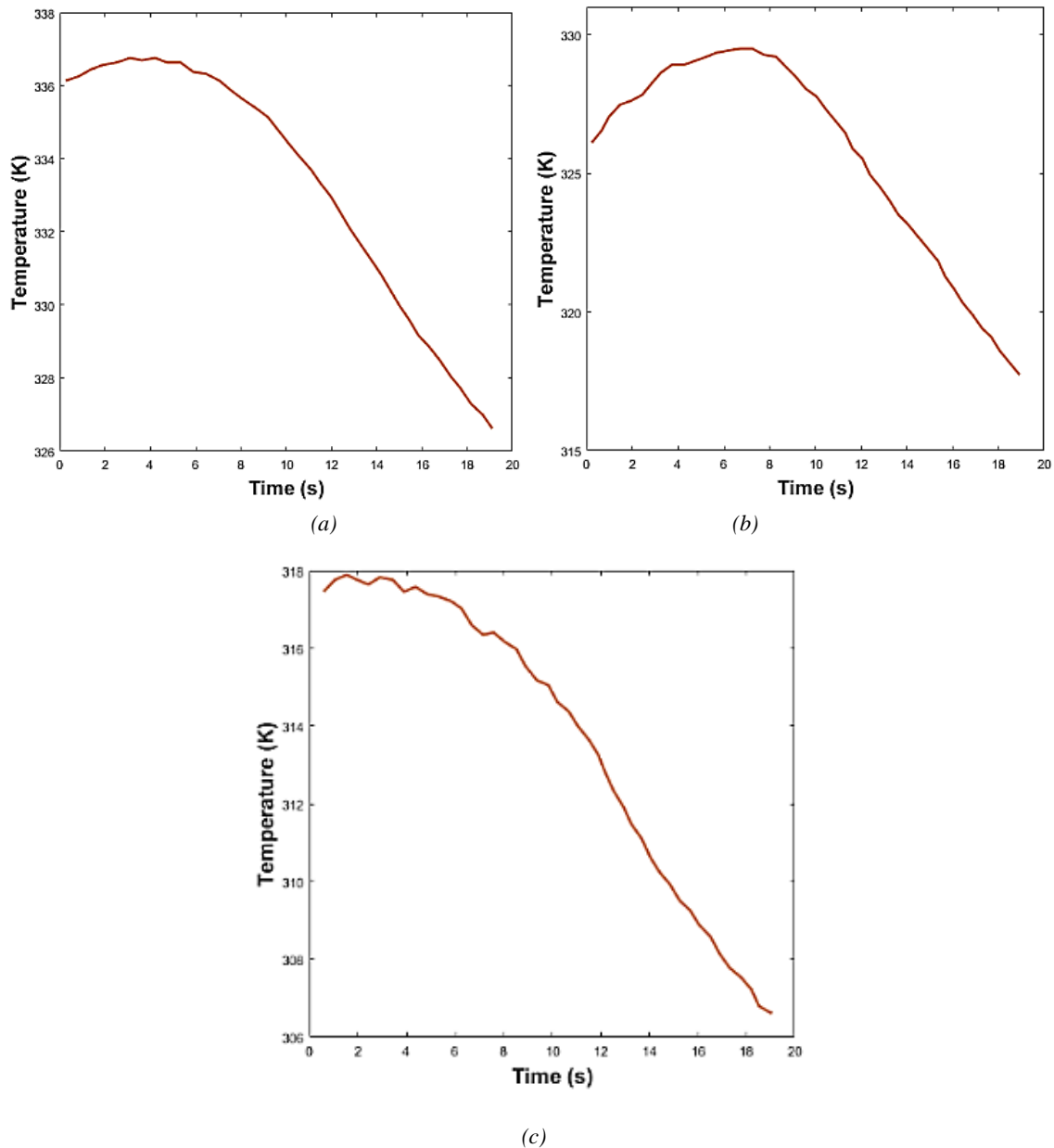


Fig. 12. Experimental curves of the temperature variation measured for a CFRP sample with three defects located at depths of $e = 0.25$ mm (a), $e = 0.5$ mm (b) and $e = 1$ mm (c) (color online)

We have compiled in table 3 the results of the neuronal model using data from experimental curves a, b, and c. Indeed, the differences between the real defect depths and those estimated by the neural network from the thermal contrast are very low, they do not exceed 7% in the worst case, perhaps this is due to small temperature fluctuations. Table 3 confirms the effectiveness of the neural model developed in estimating the defects depths inside CFRP materials.

Table 3. Comparisons between the depths estimated by the network and the real depths

Real defect depth (mm)	Estimated depth (mm)	Gap (%)
0.25	0.235	6
0.50	0.489	2
1.00	1.068	7

For future work, this accuracy can be improved by using temperature curves containing the heating and the cooling phases. Another perspective of future work is to improve the proposed neural model in order to assess the dimensions of the defect too.

4. Conclusion

In this work, a non-destructive control approach, using pulsed infrared thermography data, is established to estimate the depth of internal defects in CFRP composite materials by neural networks. A preprocessing of the network training data was done using standard thermal contrast. The principal component analysis has reduced the number of inputs processed by the neural network by using five principal components. The established neural model was tested with thermographic data (experimental and theoretical) of defects in CFRP composite for estimating their depths. The differences between defects depths real values and those estimated are very low, they do not exceed 7% in the worst case. The obtained results showed that the proposed method can be a reliable means for composite non-destructive testing.

References

- [1] G. Poelman, S. Hedayatrasa, J. Segers, J. A. C. Tellez, W. V. Paepgem, M. Kersemans, *Proceedings* **2**(8), 457 (2018).
- [2] Y. Li, W. Zhang, Z. Yang, J. Zhang, S. Tao, *Infrared Phys. Technol.* **76**, 91 (2016).
- [3] A. Elhassnaoui, A. El Ballouti, S. Sahnoun, *J. Optoelectron. Adv. M.* **15**(5-6), 447 (2013).
- [4] T. Lisle, M.-L. Pastor, C. Bouvet, P. Margueres, *Compos. Struct.* **161**, 275 (2017).
- [5] S. Marinetti et al., *Infrared Phys. Technol.* **46**(1-2), 85 (2004).
- [6] X. Maldague, *Theory and Practice of Infrared Thermography for Nondestructive Testing*, Wiley, Interscience, 2001.
- [7] L. Yuanlin, T. Qingju, B. Chiwu, M. Chen, W. Pingshan, Z. Jiansuo, *Infrared Phys. Technol.* **72**, 90 (2015).
- [8] N. Saeed, M. A. Omar, Y. Abdulrahman, *Infrared Phys. Technol.* **94**, 55 (2018).
- [9] T. H. Abraham, *Journal of the History of the Behavioral Sciences* **38**(1), 3 (2002).
- [10] N. I. E. Farhana, M. S. Abdul Majid, M. P. Paulraj, E. Ahmadhilmi, M. N. Fakhzan, A. G. Gibson, *Compos. Struct.* **144**, 96 (2016).
- [11] L. Prechelt, in *Neural Networks: Tricks of the trade*, Springer, p. 55, 1998.
- [12] G. Cybenko, *Math. Control Signals Syst.* **2**, 303 (1989).

*Corresponding author: hicham.halloua@gmail.com